Fluorescence Quantum Efficiency Enhancement in Size-Controlled 3.5 Monolayer Cadmium Telluride Nanoplatelets

Fadi AL-Shnani[†], *Chandra Sekhar M.*[†], *Carmelita Rodà*[†], *Iwan Moreels*[†,*]

[†]Department of Chemistry, Faculty of Science, Ghent University, 9000, Ghent, Belgium.

ABSTRACT

In this work, we developed a synthesis of 3.5 monolayer CdTe nanoplatelets with controlled lateral dimensions. We show that the chemical reactivity of the tellurium precursor plays an important role in achieving this. In addition, we report on the effects of additives, such as oleic acid, acetic acid and water, on the final nanoplatelet lateral dimensions and optical properties. Oleic acid and acetic acid affect the width of CdTe nanoplatelets, while water mainly affects the PL QE. We obtained an optimal combination of additives that reduces the nanoplatelet area to a minimum. Finally, after exposure of the samples to cadmium propionate, we obtained 3.5 monolayer CdTe nanoplatelets fluorescence quantum efficiency up to 12%.

Introduction

The optoelectronic and chemical properties of semiconductor nanocrystals depend on their composition, size, shape and surface functionality. Among them, cadmium telluride nanoplatelets (CdTe NPLs), with an associated bulk band gap (Eg) of 1.44 eV, are a promising material for photonic applications across the visible and near-infrared spectral range. This potential stems from the fact that CdTe NPLs, similar to CdSe NPLs, can be prepared with monodisperse thickness through colloidal methods, with spectrally narrow and tunable emission.[1] Moreover, while not investigated in-depth for CdTe NPLs yet, in general NPLs exhibit a large absorption coefficient,[2] high binding energy, giant oscillator strength and fast radiative recombination rate,[3] all promising properties for active opto-electronic devices such as phosphors for displays or luminescent solar concentrators, light-emitting diodes, or lasers.[4,5]

Colloidal synthesis is a powerful strategy to alter NPLs optoelectronic and chemical properties, yet the synthesis of high-quality CdTe NPLs is much less investigated compared to more common CdSe NPLs, and there are only few reports on the colloidal synthesis of CdTe NPLs. Initially, in 2011, Ithurria et al. reported the synthesis of zinc blende CdTe NPLs and the modelling of their optoelectronic properties.[1] Pedetti et al. then optimized this synthesis toward the formation of three different NPL populations with a thickness defined with atomic precision,[6] and with only strongly reduced contribution from other thicknesses for each sample. Still, the thickness remained limited to 4.5 monolayers for monodisperse samples. Most importantly, these zinc blende NPLs are typically grown with lateral dimensions exceeding 100 nm[1,6] and fluorescence quantum efficiencies ranging from 0.1% to 1%.[6] Only recently, Anand et al. reported zinc blende CdTe NPLs with reduced area and photoluminescence quantum efficiency (PL QE) of 9%.[7]

In addition, the Buhro[8] and Jia groups[9] reported the synthesis of wurtzite CdTe NPLs with small lateral dimensions, highlighting the key role of the Te-precursor reactivity in controlling the NPL surface extent. Specifically, the former replaced the trioctylphosphine telluride (TOPTe), typically used for the synthesis of zincblende NPLs,[6] with tris(dimethylamino)phosphine telluride (TMAPTe), while the latter used polytelluride (Te_3^{2-}, $Te_2^{2-}$and Te^{2-}) solutions in tributylphosphine (TBP). However, the full width at half maximum of the first absorption peak in wurtzite NPLs amounts to 20 nm (as extracted from the reported absorption spectrum),[8] a value much larger than the 7 nm typically reported for zinc blende NPLs.[6] Moreover, even after ligand exchange to thiolate ligands, no photoluminescence has been observed in wurtzite NPLs.[10]

In this work, we therefore focused on obtaining zinc blende 3.5 monolayer (ML) CdTe NPLs with reduced lateral dimensions. We demonstrate that, also for zinc blende NPLs, the chemical reactivity of the tellurium precursor plays an important role in controlling the NPL area. In particular, TBPTe as the most reactive precursor yields relatively small CdTe NPLs, where TOPTe and TMAPTe as less reactive precursor yields larger CdTe NPLs. To further tune the lateral dimensions, we adopted a design-of-experiments approach. This allowed for a fast optimization of the synthesis parameters, at the same time giving us insight into the main parameters that control the final properties of our 3.5 ML CdTe NPLs. Our results show that an increased oleic acid concentration decreases the area of the NPLs, while, within our explored parameter range, the acetic acid concentration produces larger NPLs when the oleic acid concentration is low, and has no significant effect when the oleic acid concentration is high. Finally, we observed an overall enhancement in the PL QE of CdTe NPLs compared to literature results,[6] with PL QE values varying between 0.6% and 4.1%. Exposure of the NPL suspensions to cadmium propionate further increases this value to the double-digit regime, reaching up to 12.5%. The PL QE enhancement correlates with time-resolved PL measurements, where we observed that the decay component associated with radiative decay, becomes more prevalent when the PL QE increases, while fast nonradiative charge trapping is reduced.

Experimental section

Chemicals. Cadmium acetate (99.997%) and tellurium powder (≥99.99%) were purchased from Sigma-Aldrich, hexadecane (99%) and ethyl acetate (99.5%) from Acros Organics. Oleic acid (OA, 90%) was purchased from Alfa Aesar, anhydride acetic acid was pushed from Merck, hexane (>99%), disolol® (ethanol, 98%) from Chem Lab. Tributylphosphine (93.5%), tris(dimethylamino)phosphine triamide (97%) and trioctylphosphine (97%) were purchased from strem. All chemicals were used without further purification.

3.5 ML CdTe NPL synthesis with different Te-precursors. Three Te-precursor solutions were prepared, consisting of 3.74 M TPBTe, 2.17 M TOPTe and 5.34 M TMAPTe. We prepared these by heating 2.32 g, 5.07 g and 1.46 g of Te at 75° C for 3 h in 1.45 mL of TBP, 2.1 mL of TOP and 1.04 mL of TMAP, respectively. Afterward the mixture was cooled to room temperature and filtered to obtain a clear solution. We added an excess of tellurium to the phosphine, and confirmed the absence of unreacted phosphine from the Te-precursors by measuring ^{31}P nuclear magnetic resonance (NMR) spectroscopy, where we only observed a single ^{31}P resonance at -14.09, -13.097 and 113.12 ppm for TBPTe, TOPTe and TMAPTe, respectively (**Figure S1**). For the NPL synthesis, a mixture of 0.5 mmol cadmium acetate, 1.15 mmol of oleic acid and 13 mL of hexadecane were inserted in a three neck-flask and the mixture was heated to 210° C under dry N_2 flow. Next, 45 µL of a 3.74 M TBPTe, (77 µL for TOPTe, 32 µL for TMAPTe) solution was diluted with 2 mL of hexadecane and cannulated to the reaction flask over the course of 2 min, after which the reaction was kept at 210 °C for 5 min. Afterward the flask was cooled with a water bath, and at 100 °C, 2 mL of oleic acid was added to quench the reaction. 10 mL of hexane was added to the reaction mixture when the temperature reached 35 °C. Another 10 mL of hexane and 5 mL of isopropanol were added, followed by centrifugation for 10 min at 4300 rpm. The NPLs precipitated under these conditions, while byproducts remained in the liquid phase. After decantation, 10 mL of hexane and 5 mL of ethyl acetate were added to the precipitated NPLs, followed by centrifugation at 3900 rpm. The liquid phase was again discarded, and CdTe NPLs were finally dispersed in hexane.

Design-of-Experiments study of 3.5 ML CdTe NPLs. To understand how to control lateral dimensions in CdTe NPLs, we followed a design-of-experiments approach, using the definitive screening design (DSD) as implemented in the JMP® software.[11] DSD is well suited to optimize input parameters when the number of variables is limited as is the case here, and requires only thirteen experiments when maximally four variables are defined. We opted to investigate the role of acetic acid (the short-chained acid), oleic acid (the long-chained acid), and water, the latter because previous work on CdSe NPLs revealed an influence on the lateral aspect ratio.[12] **Table 1** summarizes the concentration ranges for each. In a typical synthesis, 0.5 mmol of cadmium acetate, -a varying concentration of- oleic acid, acetic acid and water, and 13 mL of hexadecane were inserted in three-neck flask. The reaction flask was heated to 210 °C. Then, 45 μL of 4.84 M TBPTe solution was diluted with 2 mL hexadecane and cannulated to the reaction flask at 210 °C. The cannulation of TBPTe finished after 2 min, and the reaction was kept at 210 °C for 5 min. Afterward, reactions were quenched and samples were purified as described above.

Post synthesis Z-type ligand treatment. Cadmium propionate was synthesized from cadmium trifluoroacetate.[13] Cadmium trifluoroacetate was obtained from the reaction between CdO (4.5 mmol), trifluoroacetic acid (0.9 mmol) and trifluoroacetic anhydride (4.5 mmol) in 20 mL acetonitrile. After 15 min CdO was dissolved and the colorless solution was added to mixture of propionic acid (9 mmol), triethylamine (10.1 mmol) and 100 mL isopropanol causing to a formation of white precipitate which then was isolated and washed with (3 X 25 mL) acetone and dried overnight under vacuum.

Before ligand treatment, the samples were purified once more to further remove byproducts. NPLs were dispersed in 5 mL and was sonicated for 5 min at room temperature. 10 mL of toluene was dropped-wise on the NPL dispersion and let the NPLs dispersion stand for 60 min at room temperature. The liquid phase was decantated, and the NPLs were precipitated by centrifuging at 3900 rpm for 10 min. The final NPLs were dispersed in hexane.

For the ligand treatment, one gram of cadmium propionate was mixed with 2 mL toluene and 100 μL of 3.5 ML CdTe NPLs in hexane. We kept stirring for 24h at room temperature under inert gas conditions. Then NPLs were isolated by centrifugation at 3900 rpm for 7 min and then dispersed in 500 μL toluene.

Structural characterization. Samples for NMR spectroscopy were prepared by dilution of 90 μL Te-precursor (or associated phosphine) with 500 μL deuterated toluene. ^{31}P MMR measurements were recorded on a Bruker AVANCE II spectrometer. Samples for X-ray diffraction were prepared by dropcasting a CdTe NPL suspension on a silicon wafer. XRD patterns were acquired using Bruker D8 Discover diffractometer in Bragg−Brentano geometry (goniometer radius 280 mm) using Cu Kα radiation ($\boldsymbol{\lambda}$ = 1.54184 Å). Samples for transmission electron microscopy were prepared by drop casting a CdTe NPL suspension on a carbon supported film 200 mech copper TEM grid. Bright-field TEM images were acquired on a JEOL JEM-1011 microscope (W filament) operating at an accelerating voltage of 60 kV.

Optical spectroscopy. UV-vis absorbance spectra were recorded with a PerkinElmer Lambda 365 spectrometer. From the absorbance at 309 nm, A309, we calculated the NPL concentration c_{NPL} using the intrinsic absorption coefficient μ_i (cm^{-1}), which is calculated from bulk optical constants for CdTe (3.462 + i 9.366), the CdTe volume V_{NPL} the refractive index of the solvent (n = 1.405), and the dilution factor D applied to prepare the absorbance sample (sample length L, cm):

$$c_{\mathrm{NPL}} = \ln 10 \frac{A_{\mathrm{NPL}}}{N_A \cdot \mu_i \cdot V_{\mathrm{NPL}} \cdot L} \cdot D \qquad (1)$$

Details of the calculation of μ_i are provided in the supporting information (SI), section S1. PL spectra were collected with an Avantes spectrometer, using a 365 nm LED. The PL QE was measured using a comparative method which involves the use of a well characterized standard sample with known PL QE. We used rhodamine 6G as a reference (QE of 95% in ethanol) and the following relationship:[14]

$$QY_S = QY_R\left(\frac{I_S}{I_R}\times\frac{OD_R}{OD_S}\times\frac{n_S^2}{n_R^2}\right) \tag{2}$$

S and *R* represent the sample (CdTe NPLs) and reference (rhodamine 6G),[15,16] *I*, *OD* and *n* represent the integrated PL intensity, optical density and refractive index, respectively. Time-resolved PL traces were collected using a femtosecond laser (Spectra physics, Maitai, 80 MHz, < 100 fs) with center wavelength around 800 nm, which was frequency-doubled to 400 nm with a BBO crystal. A pulse selector (Spectra physics, Model 3980) reduced the repetition rate to 1 MHz. The PL was collected using a single-photon detector (ID Quantique, instrument response time 50 ps) connected via a multimode fiber (50 μM, NA = 0.22).

Results and discussion

A typical 3.5 monolayer CdTe NPL synthesis reported in literature is based on the hot injection of TOPTe in a solution containing cadmium acetate, oleic acid and octadecene.[6] At the end of the reaction, relatively large CdTe NPLs are formed with a PL QE of 0.1-1%. Under the assumption that a reduced lateral area may improve these PL QE values, as a first step, we investigated the influence of Te-precursor reactivity on the final NPL area (**Figure 1**).

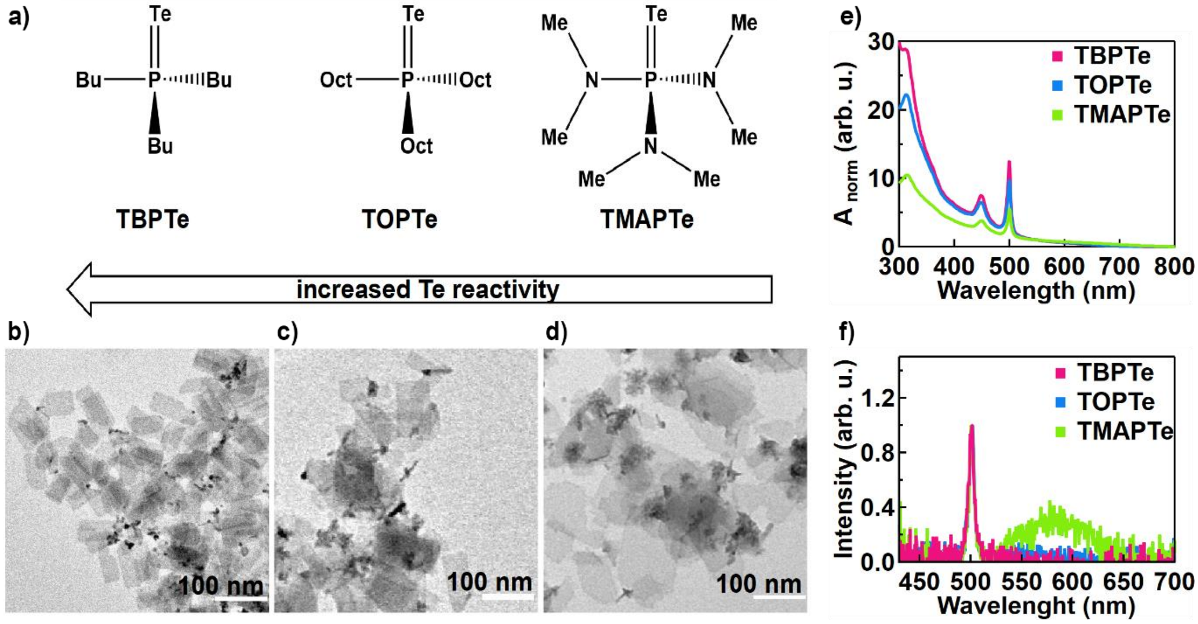

Figure 1. (a) Relative Te-precursor reactivity. (b-d) TEM images of CdTe NPLs synthesized with TBPTe, yielding 28 nm x 57 nm NPLs (b), TOPTe, yielding 45 nm x 84 nm NPLs (c), and TMAPTe, yielding 57 nm x 91 nm NPLs (d). (e) UV-Vis spectra of CdTe NPLs synthesized using the three different Te-precursors. (f) Corresponding PL spectra of the synthesized NPLs.

We used three different Te-precursors, TBPTe, TOPTe and TMAPTe, with different phosphorus substituents. Increasing their electron-donating ability stabilizes the +5 formal charge of P in the corresponding P=Te precursor, leading to a decrease of the precursor reactivity (**Figure 1a**). An XRD pattern of the sample with TBPTe as a precursor confirms that we indeed produced zinc blende NPLs (SI, **Figure S2**). **Figure 1b-d** shows representative transmission electron microscopy (TEM) images of CdTe NPLs synthetized with TBPTe, TOPTe and TMAPTe respectively. Apart from a different Te-precursor, reaction conditions were kept the same, and we measured the width and length of the resulting CdTe NPLs (Supporting Information, **Figure S3**). The resulting area clearly decreases with increasing Te-precursor reactivity, from $(5.0\pm0.5)\cdot10^3$ nm^2 for TMAPTe to $(3.7\pm0.3)\cdot10^3$ nm^2 for TOPTe, *i.e.* by a factor of two, followed by a further three-fold reduction to $(1.6\pm0.1)\cdot10^3$ nm^2 for TBPTe. Further corroborating this point, when normalizing the absorption spectra (**Figure 1e**) to the long-wavelength background, the first absorption peak, associated with the heavy hole-electron transition, is clearly more pronounced in NPLs synthesized using the Te-precursor with higher reactivity, suggesting a suppression of Rayleigh scattering in the TBPTe-based CdTe NPLs. Note that this may serve as a more qualitative assessment of NPL size, as we also observe some relatively large byproducts in the TEM images. Finally, the PL spectra show that TBPTe yields 3.5 ML CdTe NPLs with the lowest contribution of trap band emission (**Figure 1f**). Hence, we can conclude that the larger reactivity of the Te-precursor introduced by TBPTe yields smaller NPLs, with more pronounced exitonic features and a suppression of surface defects.

Next, we performed an DSD optimization of the synthesis with TBPTe. Introduced by Jones and Nachtsheim in 2011,[17] DSD can identify the input parameters, also called factors, that have a statistically significant effect on a given response, in our case the area or width of the CdTe NPLs, using a limited set of experiments. We recently applied it successfully to optimize a MoS_2 colloidal synthesis, demonstrating the potential of this approach.[18] Here we target a synthesis of 3.5 ML CdTe NPLs with small lateral dimensions and high PL QE. Our approach is based on modifying the nucleation and growth of the CdTe NPLs by varying the amount of additives such as oleic acid (OA, 0.5 - 1.8 mmol), acetic acid (AcAc, 0.0001 - 0.003 mmol) and water (H_2O, 0.00025 - 0.0025 mmol) in the reaction. We acknowledge that, using a growth temperature of 210 °C, some AcAc and H_2O will evaporate. Yet, they may also partake in a chemical equilibrium reaction (*cfr.* reference [12] and **equation (4)** below) involving also OlAc and $Cd(AcAc)_2$. Hereby changing the nature of the Cd precursor, we deemed it important to assess the influence of these parameters. As we examined three variables in our synthesis, the DSD can be limited to thirteen syntheses (**Table 1**).

Table 1. Experimental design, with the different input factors X_i, and the observed responses Y_i.

Run	X_1: OA (mmol)	X_2: AcAc (mmol)	X_3: H_2O (mmol)	Y_1: NPL width (nm)	Y_2: NPL length (nm)	Y_3: NPL area (10^3 nm2)	Y_4: PL QE (%)
1	1.15	0.003	0.0025	58	99	5.7	2.0

2	1.15	0.0001	0.00025	29	61	1.8	0.7
3	1.80	0.00155	0.00025	35	67	2. 4	2.5
4	0.50	0.00155	0.0025	47	80	3.8	1.5
5	1.80	0.0001	0.001375	21	39	0.81	2.7
6	0.50	0.003	0.001375	112	161	18.0	0.6
7	1.80	0.003	0.00025	14	27	0.38	1.9
8	0.50	0.0001	0.0025	33	59	1.9	4.1
9	1.80	0.003	0.0025	26	60	1.6	1.8
10	0.50	0.0001	0.00025	37	68	2.5	0.9
11	1.80	0.0001	0.0025	21	48	1.0	4.1
12	0.50	0.003	0.00025	76	109	8.3	0.7
13	1.150	0.00155	0.001375	36	71	2.6	2.3

Before proceeding to a detailed discussion of the influence of the input parameters X_i on the different responses Y_i, we highlight some general features of our synthesis. In particular, within our parameter space used, the width, length (SI, **Figure S4**) and area are correlated. Indeed, the aspect ratio shows little variation (**Figure 2a**), ranging only between 1.4 and 2.3, and as a result, the area scales with the width (**Figure 2b**). Hence, we can focus our further analysis on the width of the NPLs, which has the benefit that we only have to measure a single output parameter.

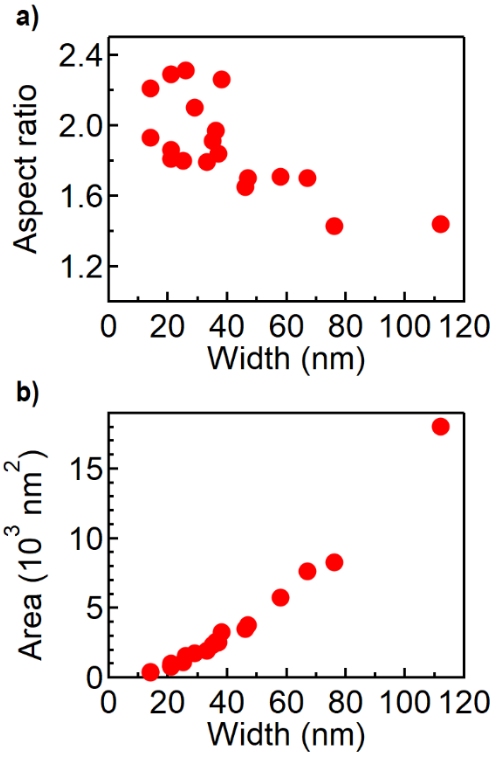

Figure 2. a) The CdTe NPL aspect ratio shows little variation when the synthesis is performed using TBPTe. b) In our synthesis parameter range, the NPL area scales with the width of the NPLs. Data include the initial 13 syntheses (**Table1**), as well as additional runs (**Table 4**).

Analyzing the influence of the input parameters on the width henceforth, *via* JMP®[11] we can construct a response surface and identify the parameters that have a statistical influence on this response, which include single factors X_i as well as two-factor products $X_i \cdot X_j$, by the so-called *p*-value. A *p*-value of 0.05 is typically taken as the threshold beyond which the associated input parameter has no influence on the response. **Table 2** shows the different *p*-values, from which we can conclude that both the concentration of AcAc and OA have an influence on the width of the CdTe NPLs, while water has not, as the *p*-value clearly exceeds 0.05.

Table 2. The calculated model coefficients and related statistical results when the NPL width is the model response.

coefficient	Term	Value	error	*p*-value
b_0	Intercept	41.9	3.2	0.0001
b_1	[OA]	-18.8	3.6	0.0006
b_2	[AcAc]	14.5	3.6	0.0031
b_3	[OA*AcAc]	-15.0	4.1	0.0049
b_4	[H_2O]	-0.6	3.8	0.8796

This leads to the following response equation for the width (Y_1) of the NPLs as a function of the concentration of OA ([OA]) and AcAc ([AcAc]):

$$Y_1 = b_0 + b_1\left(\frac{([OA]-1.15)}{0.65}\right) + b_2\left(\frac{([AcAc]-0.00155)}{0.00145}\right) + b_3\left(\frac{([OA]-1.15)}{0.65}\right)\left(\frac{([AcAc]-0.00155)}{0.00145}\right) \quad (3)$$

The values of the respective pre-factors b_i are reported in **Table 2**. To understand the role of OA and AcAc in more detail, we can visualize the response in a 2D contour plot, projecting all data for the width (**Table 1**) on this 2D plane, and plotting it as a function of [OA] and [AcAc] (**Figure 3a**).

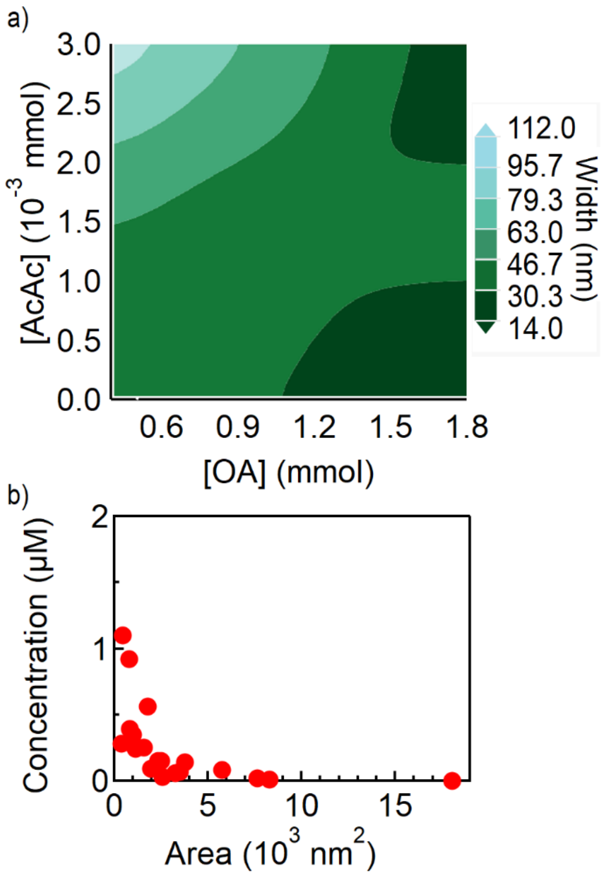

Figure 3. a) Contour plot of the NPL width as a function of concentration of excess OA and AcAc added to the synthesis. At low OA concentration, the width decreases with decreasing AcAc concentration, at high OA concentration, the AcAc concentration has only a small influence. b) The final NPL concentration in solution increases as the NPL area decreases. Data include the initial 13 syntheses (**Table1**), as well as additional runs (see **Table 3**).

The evolution of the width (and thus overall area) of the CdTe NPLs can be understood from this plot, considering that the synthesis of CdTe is initiated by mixing 0.5 mmol of Cd(AcAc)$_2$, together with OA and AcAc and heating it to 210 °C, before slowly injecting TBPTe. At this temperature, a chemical equilibrium will establish itself:

$$\mathrm{Cd(CH_3COO)_2 + 2\,C_{17}H_{33}COOH \leftrightharpoons Cd(C_{17}H_{33}COO)_2 + 2\,CH_3COOH} \tag{4}$$

Hence, for larger concentrations of AcAc and lower concentrations of OA, the equilibrium lies to the left, and we produce a relatively larger concentration of Cd(AcAc)$_2$. In this region, reducing the concentration of AcAc also leads to a reduction of NPL size. On the other hand, larger concentrations of OA or smaller concentrations of AcAc shift the equilibrium to the right, increasing the concentration of Cd(OA)$_2$. As under these conditions smaller NPLs are produced, the results suggest that under such circumstances we are extending the nucleation phase, producing more CdTe seeds, that subsequently grow into smaller NPLs. This can also be appreciated when we plot the final concentration of NPLs as a function of NPL area (**Figure 3b**, see methods, **equation 1** for calculation). Indeed, smaller NPLs are produced in larger concentrations, confirming the larger initial seed concentration and subsequent growth into smaller NPLs.

Table 3. Amounts of oleic acid, acetic acid and water used for the validation experiments of the 3.5 ML CdTe NPLs.

Run	**X_1 : OA (mmol)**	**X_2: AcAc (mmol)**	**$X3$: H_2O (mmol)**
14	1.8	0.003	0.0025
15	1.15	0.00155	0.0025
16	1.8	0.0001	0.0025
17	1.15	0.003	0.00025
18	0.5	0.00155	0.00025
19	0.5	0.003	0.0025

To confirm the accuracy of the width prediction using **equation 3**, we performed six control experiments with varying conditions (**Table 3**). From TEM images (SI, **Figure S5**) we again determined the width of the 3.5 ML CdTe NPLs. The experimental width (Width (E)) is compared to the prediction (Width (P)) of **equation 3** in (**Figure 4**). A linear fit with slope equal to one yields R^2 = 0.962, showing that we have a good correspondence between experimental and predicted values, and we can reliably vary synthesis conditions to tune the lateral sizes of 3.5 ML CdTe NPLs.

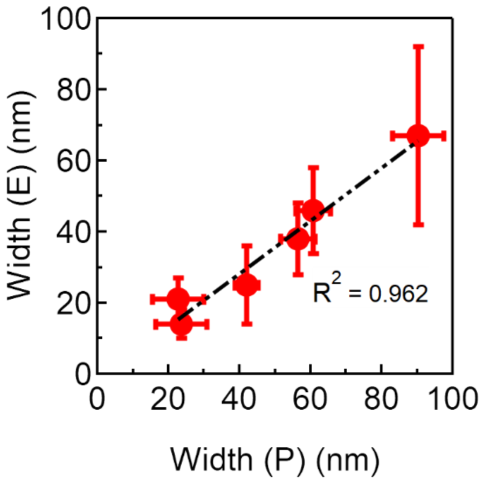

Figure 4. Experimental Width (E) plotted against predicted Width (P) for 3.5 ML CdTe NPLs synthesized using varying experimental conditions. Error bars in x- and y-direction are the calculated uncertainty (standard deviation), corresponding to the uncertainties from the three variables in the model ([OA], [AcAc] and [H_2O]), and the standard deviation from TEM width analysis, respectively.

In addition, combining results from the 13 first runs and the 6 control experiments, we observed that decreasing the lateral size from 112 nm to 14 nm in 3.5 ML CdTe NPLs impacts the confinement within these NPLs, which is reflected as a small blue shift of the spectral position of the first absorption peaks from 502 nm to 499 nm (**Figure 5a**). When plotting the PL QE as a function of NPL area (**Figure 5b**), despite a pronounced scattering of the data we observe a general upward trend of the PLQE, suggesting that reducing the area indeed increases the PL QE.

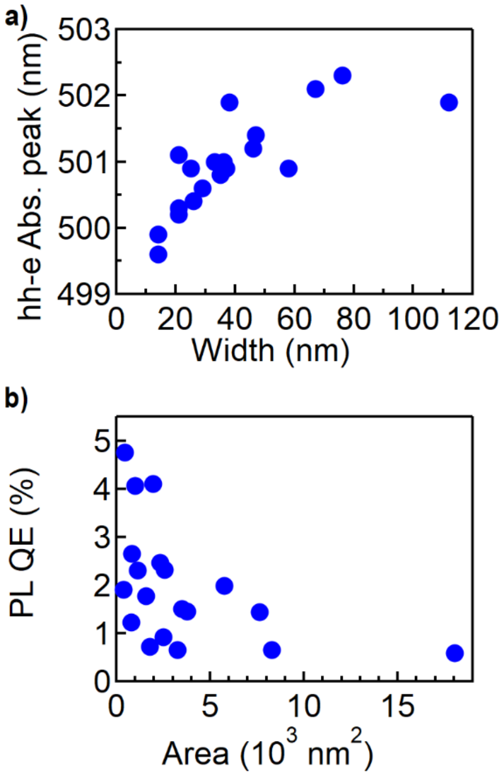

Figure 5. a) Correlation between the NPL width and the heavy hole-electron absorption wavelength. b) Correlation between the NPL area and PL QE.

We therefore further investigated the main factors affecting the PL QE. The response model equation for the PL QE (Y_4) reads:

$$Y_4 = c_0 + c_1\left(\frac{([\mathrm{OA}]-1.15)}{0.65}\right) + c_2\left(\frac{([\mathrm{AcAc}]-0.00155)}{0.00145}\right) + c_3\left(\frac{([\mathrm{H2O}]-0.001375)}{0.001125}\right) + c_4\left(\frac{([\mathrm{AcAc}]-0.00155)}{0.00145}\right)\left(\frac{([\mathrm{H2O}]-0.001375)}{0.001125}\right) \quad (5)$$

Table 4 presents the calculated model coefficients and related statistical results. Interestingly, in addition to the concentration of oleic acid and acetic acid, also water plays a role here. **Figure 6** shows 2D plots of the PL QE as a function of these concentrations. A high concentration of oleic acid and low concentration of acetic acid increases the PL QE (**Figure 6a**). Since these conditions match the synthesis parameters to obtain narrow widths, we can conclude that smaller NPLs can lead to higher PL QE. Interestingly, in contrast to CdSe NPLs,[12] the inclusion of water did not influence the lateral dimensions (**Table 2**, **equation (3)**), however, an increase of the PL QE is predicted for higher concentration of water (**Figure 6b**), presumably due to passivation of surface defects via $Cd(OH)_x$.

Table 4. The calculated model coefficients and related statistical results when the PL QE is the model response.

coefficient	term	value	error	p-value
c_0	Intercept	1.97	0.16	<.0001
c_1	[OA]	0.51	0.18	0.0216
c_2	[AcAc]	-0.56	0.18	0.0153
c_3	[H2O]	0.67	0.18	0.0059
c_4	[AcAc][H2O]	-0.66	0.20	0.0111

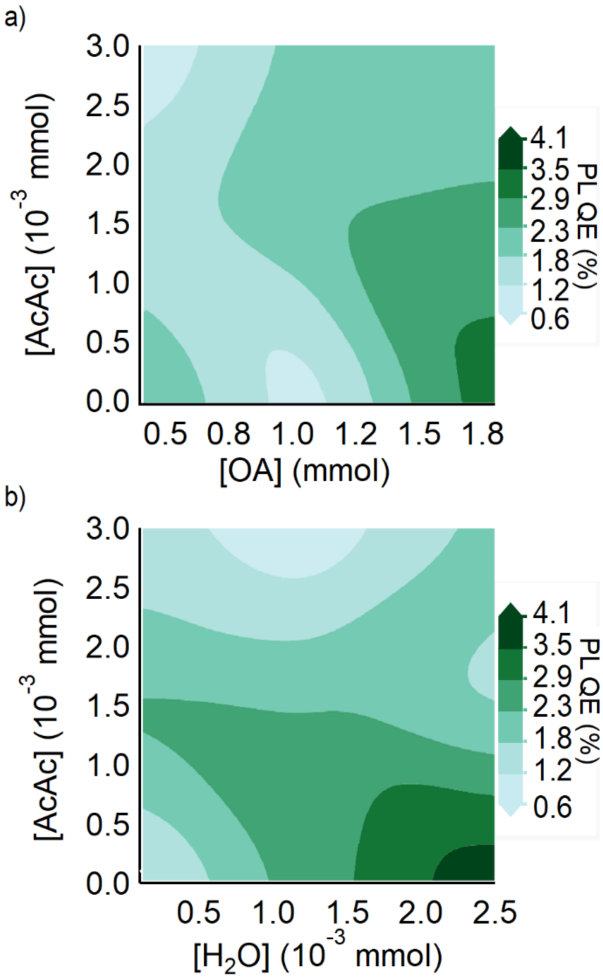

Figure 6. a) Contour plot showing the influence of acetic acid and oleic acid on the NPL PL QE. b) Contour plot showing the influence of acetic acid and water on the NPL PL QE. From

both panels, we can appreciate that a high PL QE is obtained for low concentration of acetic acid, and high concentration of oleic acid and water.

After establishing a concrete understanding on the conditions that affect the size and PL QE of 3.5 ML CdTe NPLs, we investigated the optimal synthesis conditions to obtain small width and high PL QE. To this aim, we set the model desirability to minimize the width response (Y_1) and maximize the PL QE response (Y_4). The model suggests 1.8 mmol [OA], 0.0001 mmol [AcAc] and 0.0025 mmol [H_2O] as optimal concentrations. For these conditions, it predicts a width of 24 ± 7 nm, and a PL QE of 4.3 ± 2.3 %. We synthesized three different batches of CdTe NPLs following the suggested conditions. **Figure S6a-c** shows representative TEM images of the CdTe NPLs, from which the lateral dimensions were extracted (see **Figure S6d-f** for associated histograms). The associated absorption and PL spectra are shown in **Figure S6g-i**. The width and length, as well as the PL QE of each sample are reported in **Table S1**. Clearly, experimental values align well with the prediction from **equations (3)** and **(5)**, especially considering that the PL QE model predicts a fairly large standard deviation.

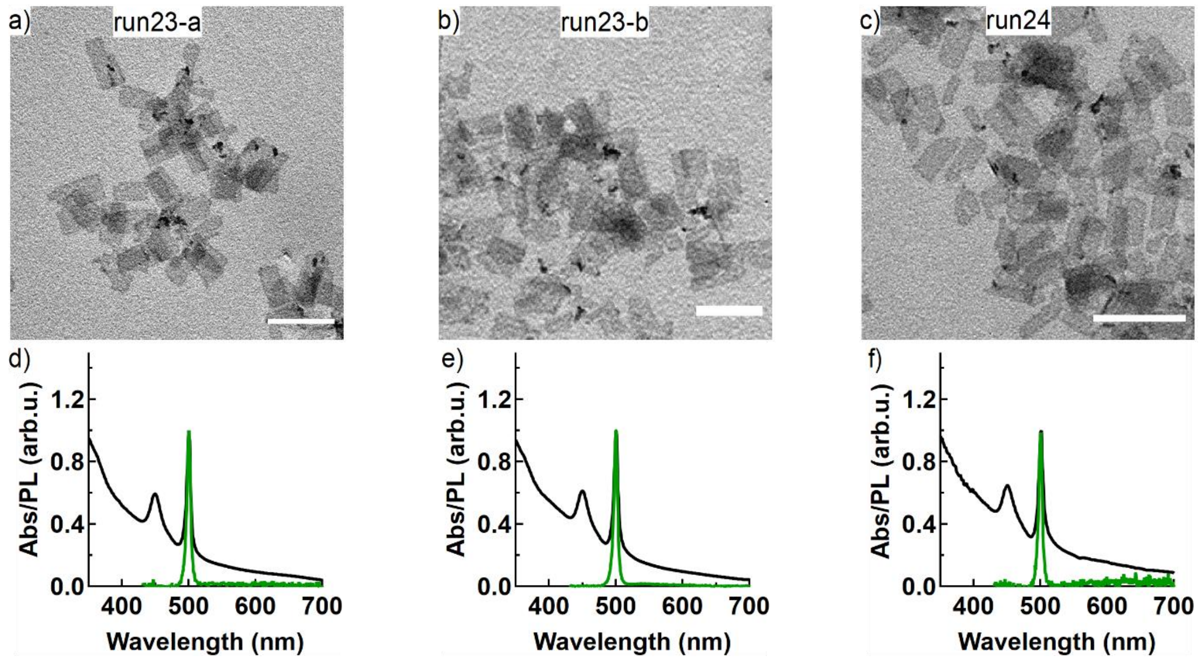

Figure 7. (a-c) TEM images of 3.5 ML CdTe NPLs synthesized under the optimal conditions (scale bar 100 nm). (d-f) Absorbance and PL spectra, taken after Cd-propionate treatment.

Table 5. CdTe NPL length and width, including size dispersion, and PL QE before and after Cd-propionate exposure. For batch 23, we repeated the ligand treatment twice to verify reproducibility. However, batch-to-batch variation can still be observed, as evidenced by comparison of batch 23 and 24.

Run	Length (nm)	Width (nm)	PL QE (%) before exposure	PL QE (%) after exposure

23-a	36 ± 10	16 ± 5	1.5	12.3
23-b	38 ± 10	14 ± 5	1.5	11.2
24	44 ± 11	18 ± 4	1.0	6.9

To further enhance the PL QE, we exposed the CdTe NPLs to a Z-type ligand, more specifically cadmium propionate. We mixed 1 g of Cd-proprionate with 100 µL of NPLs dispersed in hexane in 2 mL of toluene, and stirred this overnight under inert atmosphere. This treatment increased the PL QE, and allowed to reach values up to 12.5 % (**Figure S6**, **Table S1**). However, a second PL peak was discerned in the PL spectra, at a spectral position that agrees with 4.5 ML NPLs (**Figure S6g-i)**. This indicates that one purification step is not sufficient to eliminate the thicker NPLs. We synthesized two additional batches (run23 and run24) of CdTe NPLs following the optimal conditions suggested by the CdTe model, and we purified the NPLs once more, as described in the experimental section. The final NPLs were dispersed in hexane and again exposed to a Z-Type ligand. The corresponding TEM images, absorption and PL spectra are shown in **Figure 7a-f**. The second PL peak attributed to the fractions of thicker NPLs is no longer present in the PL spectra (**Figure 7d-f**), indicating monodisperse samples. We also verified the lateral dimensions of the NPLs (see **Figure S7** for the associated histograms) and we report the width, the length and PL QE before and after the Z-type ligand exposure (**Table 5**). The lateral dimensions are in line with the model predictions, and the PL QE is again enhanced up to 11-12%.

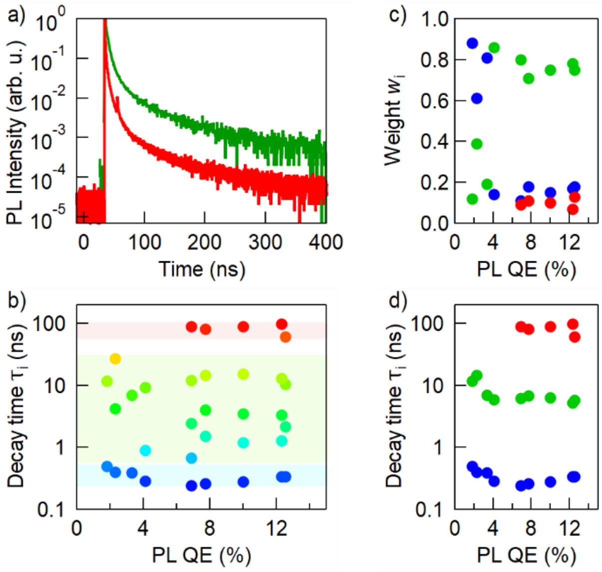

Figure 8. a) PL decay traces of 3.5ML CdTe (red) and 4.5 ML CdSe (green) NPLs, which have similar band gap. The CdTe PL decays faster, with a lower-intensity contribution from delayed emission. b) Decay times extracted from a multiexponential fit to the PL decay traces (see also SI, **Figure S8**, **Table S2**), as a function of the PL QE of the samples. We can discern fast trapping (blue region), delayed emission (red region), and components associated with the radiative decay of band-edge exciton (green region). c) Weight of the trapping (blue), decreasing with increasing PL QE, radiative (green), increasing with increasing PL QE, and

delayed emission component (red). d) Associated lifetime of the trapping (blue) component, effective lifetime of the radiative recombination (green), and delayed emission (red).

Now that we have produced a series of CdTe NPLs with PL QE that spans an order of magnitude, we can examine the time-resolved fluorescence properties in more detail. **Figure 8a** shows a typical CdTe PL decay trace (12.3% PL QE, red trace), and a typical trace of 4.5 ML CdSe NPLs (26% PL QE, green trace).[19] Time-resolved PL decay traces of the different CdTe samples where fitted with a multiexponential decay function, requiring up to five decay components to accurately fit the decay (SI, **Figure S8** and **Table S2**). Therefore, individual components bear no meaning, however, when plotting the resulting lifetimes as a function of PL QE, we can discern three regimes (**Figure 8b**). A decay component with lifetime below 500 ps (blue area), with decreasing weight for higher PL QE (**Figure 8c**, blue dots), can be assigned to fast trapping. A decay component with lifetime approaching 100 ns (**Figure 8b**, red area) and weight of about 10 % (**Figure 8c**, red dots) can be assigned to shallow carrier trapping and delayed emission. Finally, the remaining components have a lifetime ranging from about 1 ns to 30 ns (**Figure 8b**, green area), and are assigned to the prompt exciton recombination process. An area-weighted average lifetime and total weight are calculated for the latter, resulting in **Figure 8d**, green dots. This shows that the effective lifetime converges to 6.0 ns at high PL QE, dominating the overall PL decay with a weight of about 75 %. We can also compare our data for 3.5 ML CdTe NPLs with PL QE of 12.3 % to 4.5 ML CdSe NPLs that a similar band gap and a PL QE of 26 % (508 nm absorption peak, **Figure 8a**, green trace).[19] A fit to the decay trace shows that the prompt emission in CdSe NPLs (SI, **Figure S8** and **Table S3** for fit components) has an area-weighted lifetime of 10.6 ns, about a factor of two larger than CdTe NPLs. For completeness, a calculation of the amplitude-averaged lifetime, as was done previously for CdSe,[19] yields 3.3 ns for CdTe NPLs and 4.9 ns for CdSe NPLs, i.e. the same emission rate enhancement in CdTe compared to CdSe with a similar band gap is observed from these values. In addition, the onset of delayed emission occurs at about an order of magnitude lower count rate for CdTe NPLs. Both results strongly indicate that CdTe NPLs have better prospects as fast and monoexponentially decaying fluorescence emitters compared to CdSe NPLs.

Conclusions

We demonstrated a DSD optimized synthesis of 3.5 ML CdTe NPLs toward smaller areas (*ca.* 19 x 41 nm in optimized synthesis) and PL QE entering the double-digit regime (highest value of about 12%). We also showed that the Te precursor reactivity plays a key role in the size reduction, yielding smallest NPLs for TBPTe. Additionally, we elucidated the effects of oleic acid, acetic acid, water and cadmium propionate on the structural and optical properties. The modeling shows that oleic acid causes a decrease in the width of CdTe NPLs, while acetic acid has the opposite effect, yet only when the oleic acid concentration is low. The addition of water, and more importantly, the exposure to cadmium propionate post synthesis, allow us to increase the PL QE. CdTe NPLs are faster emitters compared to CdSe NPLs with similar band gap, which offers prospects for future comparative studies of both material compositions, as well as applications in light-emitting diodes,[20–23] lasers,[23–25] or ultrafast scintillators.[7,26]

ASSOCIATED CONTENT

Supporting Information. Calculation of the intrinsic absorption coefficient of CdTe nanoplatelets, XRD pattern of CdTe NPLs, TEM images and size analysis, PL decay fitting. The following files are available free of charge.

AUTHOR INFORMATION

Corresponding Author

Iwan Moreels - Department of Chemistry, Faculty of Science, Ghent University, 9000, Ghent, Belgium; orcid.org/0000-0003-3998-7618;
Email: iwan.moreels@ugent.be

Authors

Iwan Moreels - Department of Chemistry, Faculty of Science, Ghent University, 9000, Ghent, Belgium; orcid.org/0000-0003-3998-7618

Fadi AL-Shnani - Department of Chemistry, Faculty of Science, Ghent University, 9000, Ghent, Belgium; orcid.org/0000-0002-7961-806X

Chandra Sekhar M.- Department of Chemistry, Faculty of Science, Ghent University, 9000, Ghent, Belgium; orcid.org/ 0000-0002-6836-8907

Carmelita Rodà - Department of Chemistry, Faculty of Science, Ghent University, 9000, Ghent, Belgium; orcid.org/ 0000-0003-0581-3126

Author Contributions

The manuscript was written through contributions of all authors. All authors have given approval to the final version of the manuscript.

Funding Sources

This project has received funding from the UGent BOF GOA (grant agreement No. GOA01G01019 MANAWORK) and from the European Research Council under the European Union’s Horizon 2020 research and innovation program (grant agreement No. 714876 PHOCONA). We thank the NMR expertise centre (Ghent University) for providing support and access to its NMR infrastructure. TEM measurements were performed at the UGent TEM Core Facility.

REFERENCES

(1) Ithurria, S.; Tessier, M. D.; Mahler, B.; Lobo, R. P. S. M.; Dubertret, B.; Efros, A. L. Colloidal Nanoplatelets with Two-Dimensional Electronic Structure. *Nature Materials* **2011**, *10* (12), 936–941.

(2) Achtstein, A. W.; Antanovich, A.; Prudnikau, A.; Scott, R.; Woggon, U.; Artemyev, M. Linear Absorption in CdSe Nanoplates: Thickness and Lateral Size Dependency of the Intrinsic Absorption. *J. Phys. Chem. C* **2015**, *119* (34), 20156–20161. https://doi.org/10.1021/acs.jpcc.5b06208.

(3) Naeem, A.; Masia, F.; Christodoulou, S.; Moreels, I.; Borri, P.; Langbein, W. Giant Exciton Oscillator Strength and Radiatively Limited Dephasing in Two-Dimensional Platelets. *Physical Review B - Condensed Matter and Materials Physics* **2015**, *91* (12), 8–12. https://doi.org/10.1103/PhysRevB.91.121302.

(4) Zhang, J.; Sun, Y.; Ye, S.; Song, J.; Qu, J. Heterostructures in Two-Dimensional CdSe Nanoplatelets: Synthesis, Optical Properties, and Applications. *Chem. Mater.* **2020**, *32* (22), 9490–9507. https://doi.org/10.1021/acs.chemmater.0c02593.

(5) Yu, J.; Chen, R. Optical Properties and Applications of Two-Dimensional CdSe Nanoplatelets. *InfoMat* **2020**, *2* (5), 905–927. https://doi.org/10.1002/inf2.12106.

(6) Pedetti, S.; Nadal, B.; Lhuillier, E.; Mahler, B.; Bouet, C.; Abécassis, B.; Xu, X.; Dubertret, B. Optimized Synthesis of CdTe Nanoplatelets and Photoresponse of CdTe Nanoplatelets Films. *Chemistry of Materials* **2013**, *25* (12), 2455–2462. https://doi.org/10.1021/cm4006844.

(7) Anand, A.; Zaffalon, M. L.; Cova, F.; Pinchetti, V.; Khan, A. H.; Carulli, F.; Brescia, R.; Meinardi, F.; Moreels, I.; Brovelli, S. Optical and Scintillation Properties of Record-Efficiency CdTe Nanoplatelets toward Radiation Detection Applications. *Nano Lett.* **2022**, *22*, 8900–8907. https://doi.org/10.1021/acs.nanolett.2c02975.

(8) Sun, H.; Wang, F.; Buhro, W. E. Tellurium Precursor for Nanocrystal Synthesis: Tris(Dimethylamino)Phosphine Telluride. *ACS Nano* **2018**, *12*, 12393–12400. https://doi.org/10.1021/acsnano.8b06468.

(9) Wang, F.; Javaid, S.; Chen, W.; Wang, A.; Buntine, M. A.; Jia, G. Synthesis of Atomically Thin CdTe Nanoplatelets by Using Polytelluride Tellurium Precursors. *Australian Journal of Chemistry* **2021**, *74* (3), 179–185. https://doi.org/10.1071/CH20174.

(10) Sun, H.; Buhro, W. E. Contrasting Ligand-Exchange Behavior of Wurtzite and Zinc-Blende Cadmium Telluride Nanoplatelets. *Chem. Mater.* **2021**, *33* (5), 1683–1697. https://doi.org/10.1021/acs.chemmater.0c04247.

(11) JMP®, Version 16.1.0. SAS Institute Inc., Cary, NC, 1989–2021.

(12) Bertrand, G. H. V.; Polovitsyn, A.; Christodoulou, S.; Khan, A. H.; Moreels, I. Shape Control of Zincblende CdSe Nanoplatelets. *Chemical Communications* **2016**, *52* (80), 11975–11978. https://doi.org/10.1039/c6cc05705e.

(13) Hendricks, M. P.; Campos, M. P.; Cleveland, G. T.; Plante, I. J.-L.; Owen, J. S. A Tunable Library of Substituted Thiourea Precursors to Metal Sulfide Nanocrystals. *Science* **2015**, *348* (6240), 1226–1230. https://doi.org/10.1126/science.aaa2951.

(14) Chandra Sekhar, M.; De, A.; Hossain, S. S.; Samanta, A. Roles of the Methyl and Methylene Groups of Mercapto Acids in the Photoluminescence Efficiency and Carrier Trapping Dynamics of CdTe QDs. *Physical Chemistry Chemical Physics* **2017**, *19* (2), 1536–1542. https://doi.org/10.1039/c6cp07211a.

(15) Brouwer, A. M. Standards for Photoluminescence Quantum Yield Measurements in Solution (IUPAC Technical Report). *Pure and Applied Chemistry* **2011**, *83* (12), 2213–2228. https://doi.org/10.1351/PAC-REP-10-09-31.

(16) Fischer, M.; Georges, J. Fluorescence Quantum Yield of Rhodamine 6G in Ethanol as a Function of Concentration Using Thermal Lens Spectrometry. *Chemical Physics Letters* **1996**, *260* (1–2), 115–118. https://doi.org/10.1016/0009-2614(96)00838-X.

(17) Jones, B.; Nachtsheim, C. J. A Class of Three-Level Designs for Definitive Screening in the Presence of Second-Order Effects. *Journal of Quality Technology* **2011**, *43* (1), 1–15. https://doi.org/10.1080/00224065.2011.11917841.

(18) Pippia, G.; Rousaki, A.; Barbone, M.; Billet, J.; Brescia, R.; Polovitsyn, A.; Martín-García, B.; Prato, M.; De Boni, F.; Petrić, M. M.; Ben Mhenni, A.; Van Driessche, I.; Vandenabeele, P.; Müller, K.; Moreels, I. Colloidal Continuous Injection Synthesis of Fluorescent MoX2 (X = S, Se) Nanosheets as a First Step Toward Photonic Applications. *ACS Appl. Nano Mater.* **2022**, *5* (8), 10311–10320. https://doi.org/10.1021/acsanm.2c01470.

(19) Christodoulou, S.; Climente, J. I.; Planelles, J.; Brescia, R.; Prato, M.; Martín-García, B.; Khan, A. H.; Moreels, I. Chloride-Induced Thickness Control in CdSe Nanoplatelets. *Nano Lett.* **2018**, *18* (10), 6248–6254. https://doi.org/10.1021/acs.nanolett.8b02361.

(20) Giovanella, U.; Pasini, M.; Lorenzon, M.; Galeotti, F.; Lucchi, C.; Meinardi, F.; Luzzati, S.; Dubertret, B.; Brovelli, S. Efficient Solution-Processed Nanoplatelet-Based Light-Emitting Diodes with High Operational Stability in Air. *Nano Lett.* **2018**, *18*, 3441–3448. https://doi.org/10.1021/acs.nanolett.8b00456.

(21) İzmir, M.; Sharma, A.; Shendre, S.; Durmusoglu, E. G.; Sharma, V. K.; Shabani, F.; Baruj, H. D.; Delikanli, S.; Sharma, M.; Demir, H. V. Blue-Emitting CdSe Nanoplatelets Enabled by Sulfur-Alloyed Heterostructures for Light-Emitting Diodes with Low Turn-on Voltage. *ACS Appl. Nano Mater.* **2022**, *5* (1), 1367–1376. https://doi.org/10.1021/acsanm.1c03939.

(22) Hu, A.; Bai, P.; Zhu, Y.; Tang, Z.; Xiao, L.; Gao, Y. Controlled Core/Crown Growth Enables Blue-Emitting Colloidal Nanoplatelets with Efficient and Pure Photoluminescence. *Small* **2022**, *18* (44), 2204120. https://doi.org/10.1002/smll.202204120.

(23) Kelestemur, Y.; Shynkarenko, Y.; Anni, M.; Yakunin, S.; De Giorgi, M. L.; Kovalenko, M. V. Colloidal CdSe Quantum Wells with Graded Shell Composition for Low-Threshold Amplified Spontaneous Emission and Highly Efficient Electroluminescence. *ACS Nano* **2019**, *13*, 13899–13909. https://doi.org/10.1021/acsnano.9b05313.

(24) Zhang, L.; Yang, H.; Yu, B.; Tang, Y.; Zhang, C.; Wang, X.; Xiao, M.; Cui, Y.; Zhang, J. Low-Threshold Amplified Spontaneous Emission and Lasing from Thick-Shell CdSe/CdS Core/Shell Nanoplatelets Enabled by High-Temperature Growth. *Advanced Optical Materials* **2020**, *8* (4), 1901615. https://doi.org/10.1002/adom.201901615.

(25) Duan, R.; Zhang, Z.; Xiao, L.; Zhao, X.; Thung, Y. T.; Ding, L.; Liu, Z.; Yang, J.; Ta, V. D.; Sun, H. Ultralow-Threshold and High-Quality Whispering-Gallery-Mode Lasing from Colloidal Core/Hybrid-Shell Quantum Wells. *Advanced Materials* **2022**, *34* (13), 2108884. https://doi.org/10.1002/adma.202108884.

(26) Turtos, R. M.; Gundacker, S.; Omelkov, S.; Mahler, B.; Khan, A. H.; Saaring, J.; Meng, Z.; Vasil'ev, A.; Dujardin, C.; Kirm, M.; Moreels, I.; Auffray, E.; Lecoq, P. On the Use of CdSe Scintillating Nanoplatelets as Time Taggers for High-Energy Gamma Detection. *npj 2D Mater Appl* **2019**, *3* (1), 1–10. https://doi.org/10.1038/s41699-019-0120-8.

TABLE OF CONTENTS FIGURE